Title
INFLUENCE OF QUENCHING CONDITIONS ON VACANCY LOOPS IN ALUMINUM

Author
Das, Gobinda.

Publication Date
1964

UCRL-11188

University of California

Ernest O. Lawrence Radiation Laboratory

INFLUENCE OF QUENCHING CONDITIONS ON VACANCY LOOPS IN ALUMINUM

Berkeley, California

DISCLAIMER

Research and Development

UCRL-11188
UC-25 Metals,
Ceramics and
Materials

UNIVERSITY OF CALIFORNIA

Lawrence Radiation Laboratory
Berkeley, California

AEC Contract No. W-7405-eng-48

INFLUENCE OF QUENCHING CONDITIONS ON VACANCY LOOPS IN ALUMINUM

Gobinda Das

(M. S. Thesis)

January, 1964

Printed in USA. Price $1.25. Available from the
Office of Technical Services
U. S. Department of Commerce
Washington 25, D.C.

UCRL-11188

INFLUENCE OF QUENCHING CONDITIONS ON VACANCY LOOPS IN ALUMINUM

Gobinda Das

Inorganic Materials Research Division, Lawrence Radiation Laboratory
and Department of Mineral Technology, University of California
Berkeley, California

Abstract

Great differences in the substructure of quenched and aged 99.999% purity aluminum were caused by varying the thickness of specimens at the time of quenching even though all other important variables like quenching temperature, aging temperature, and time and purity were kept constant. The thickness of the specimens was varied within the range 25 to 400 microns. All specimens were quenched from 543°C into water at 40°C and aged at 40°C for 5 minutes. The size of dislocation loops resulting from clustering of excess vacancies progressively increased and their density decreased with increasing thickness of the specimens. In the thinner specimens the loops were primarily faulted with Burgers vector $\frac{a}{3}[111]$ while in the thicker specimens perfect $\frac{a}{2}[110]$ loops predominated. For the 400μ specimens nearly all loops were perfect and diamond shaped with all four sides lying on {111} planes. The habit plane of the diamond shaped loops was approximately {023}. The concentration of vacancies that was necessary to account for the size and density of loops was approximately independent of specimen thickness.

Introduction

In pure metals at elevated temperatures, vacancies exist in thermal equilibrium in appreciable concentration. A large supersaturation of vacancies can be frozen in by quenching rapidly from a high to a temperature low enough to prevent diffusion. The concentration of vacant lattice sites 'c' which is frozen-in depends on the quenching temperature and it is given by:

$$c = A \exp\left(\frac{-E_f}{kT}\right)$$

where A is an entropy factor (~1)

E_f is the energy of formation of vacancy

k is the Boltzmann Contrast

T is the temperature in °K.

When pure aluminum is quenched from 600°C to 0°C, a supersaturation of the order of 10^{-4} can be obtained.

The presence of quenched-in vacancies causes an increase in electrical resistivity. Determination of concentration of vacancies after quenching can be done by electrical resistivity measurements. Measurements of resistivity after quenching have made it possible to estimate the energy of formation of a vacancy. Bradshaw and Pearson,[1] Federighi,[2] De Sorbo and Turnbull[3] reported E_f = 0.76 ev, 0.74 ev, and 0.79 ev for aluminum.

Vacancy concentration and estimates of energy of formation can also be obtained from careful dilatometric experiments. Takamura[4] observed contraction in length of quenched gold specimens during annealing at room temperature and interpreted this in terms of vacancies. He reported E_f = 0.98 ev for gold.

Quenched-in defects also affect the mechanical properties of metals. Quench-hardening, i.e., an increase in yield strength in quenched and aged pure metals has been reported by Meshii and Kauffmann[5] and by Maddin and Cottrell.[6]

Excess vacancies introduced by quenching anneal out during aging. There are three ways in which they can be removed: (1) migration to an external surface, (2) precipitation on edge and screw dislocations, (3) clustering to form small voids which may collapse to form dislocation loops.

The mechanism of loop formation is not yet well understood. Frank (1950)[7] suggested that loops might be formed due to collapse of vacancy discs in {111} planes in fcc metals. The result is formation of a closed dislocation loop having a Burgers vector $\frac{1}{3}[111]$ normal to the plane of the loop.

Kuhlmann-Wilsdorf and Wilsdorf[8] suggested that vacancies aggregate into three dimensional clusters, containing few to thousand vacancies, before collapsing into dislocation loops. These clusters were thought to be initially spherical or ellipsoidal in shape and collapse, spherical or ellipsoidal voids → loop, was assumed to take place initially due to elastic deformation of the material. Flattening of voids was due to surface diffusion from pole to equator. When the void was only 2 to 3 atoms thick, coalescence of adjacent close-packed layers could take place giving rise to the formation of loops.

Small angle scattering experiments on quenched copper by Chik and Seeger[10] and by Galligan and Washburn[9] also suggest that voids are formed prior to formation of dislocation loops. Direct observation of voids of 80 Å diameter in copper was also reported by Seeger et al.[10]

Stacking fault energy seems to play an important role in determining the type of substructure which is observed in quenched and aged fcc pure metals by transmission electron microscopy. Three different types of defects are commonly observed:

(1) Frank-sessile dislocation loop surrounding a region of stacking fault (Burgers vector $\frac{1}{3}[111]$ normal to the plane of the loop). These defects were observed in aluminum by Washburn and Vandervoort,[14] Cotterill and Segall[15] and Yoshida et al.[16]

(2) Stacking fault tetrahedra with stair rod at each edge.

A Frank-sessile dislocation, because it has relatively large Burgers vector, will tend to dissociate into a low energy stair-rod dislocation and a Shockley partial dislocation on an intersecting slip plane, by the reaction,

$$\underset{\text{Frank Sessile}}{\frac{1}{3}[111]} = \underset{\text{Stair Rod}}{\frac{1}{6}[101]} + \underset{\text{Shockley Partial}}{\frac{1}{6}[121]}$$

Shockley partials formed in this way on the three intersecting {111} planes are able to move away from the stair rod dislocations and attract each other to form three new stair rods along the <110> directions by reactions of the type

$$\underset{\text{Shockley Partial}}{\frac{1}{6}[121]} + \frac{1}{6}[\bar{1}\bar{1}2] = \underset{\text{Stair Rod}}{\frac{1}{6}[01\bar{1}]}$$

A stacking fault tetrahedron is thus obtained with edges parallel to <110> directions. These were first observed in quenched gold, an fcc metal of low stacking fault energy, by Hirsch and Silcox.[13]

(3) Perfect prismatic loops.

In metals of high stacking fault energy like aluminum, a disc of vacancies aggregated on a {111} plane besides collapsing also undergoes a shear movement of $\frac{1}{6}[121]$ type, resulting in a perfect prismatic loop which has a Burgers vector $\frac{1}{2}[110]$ not lying at right angles to the plane of the loop.

$\frac{1}{3}[111]$	+	$\frac{1}{6}[11\bar{2}]$	=	$\frac{1}{2}[110]$
Frank Sessile		Shockley Partial		Prismatic Dislocation

This was first predicted by Kuhlmann-Wilsdorf[11] and reported by Hirsch et al.[12]

Although in a general way the types of defects observed correlate with the stacking fault energy of the material under observation, this is not always the case. In aluminum the stacking fault energy is believed to be as high as 150-200 ergs/cm^2. It was first assumed that because of such high stacking fault energy it would be possible to nucleate a Shockley partial loop in the region of stacking fault which sweeps away the stacking fault and recombines with the Shockley partial to form a perfect prismatic loop with a Burgers vector $\frac{1}{2}[110]$. The above theory was put forward to explain the observations of perfect prismatic loops in quenched polycrystalline aluminum by Hirsch et al.[12] and later by Kuhlmann-Wilsdorf and Wilsdorf.[8] More recently it has been found that for pure aluminum the predominant type of defect is not the perfect loops but is the stacking fault loop. Electron diffraction contrast experiments carried out by Strudel and Washburn[17] proved that 99% of the loops, 150-250 Å in diameter in quenched and aged single crystals of 99.999% pure aluminum were faulted in nature. These

results suggest that early experiments were influenced by other factors.

Annealing experiments by Yoshida et al.[16] showed that stacking fault loops do not transform to perfect loops even at high temperatures. When the temperature reaches about 175°C they shrink in size by emission of vacancies but remain imperfect until they disappear.

Calculations by Saada[18] have explained the stability of stacking fault loops even in metals of high stacking fault energy like aluminum. By considering the relative energies of the two types of defect as a function of their size, and by taking into account the difficulty of nucleating a loop of Shockley partial within the stacking fault of an imperfect loop, it was shown that the critical value of stacking fault energy γc above which spontaneous transformation of an imperfect loop to a perfect loop is possible is ~350 ergs/cm^2 for aluminum. Estimates of the stacking fault energy of aluminum are below γc. As a result Frank-sessile loops should continue to grow above the critical size at which the energy of a perfect loop would be smaller. These calculations suggest that perfect loops that are observed in aluminum may be formed by other mechanisms such as breaking of helices or coalescence of vacancies on planes other than {111}.

Impurity content has been shown to play a role in determining the type of loop that is formed. Cotterill and Segall[15] reported all Frank-sessile loops with zone refined 99.9999% pure aluminum. The same result could also be obtained by multiple quenching of 99.995% pure aluminum. Repeated quenching therefore produces an effect similar to that produced by increased purity. It has been suggested that purification actually occurs due to sweeping away of certain impurity atoms by vacancies as they anneal out to the surface. Some impurity atoms have high binding energy with vacancies.

In metals with only nominal purity, these solute atoms may act as sites for heterogeneous precipitates of vacancies, resulting in a type of vacancy cluster that leads to the formation of perfect prismatic loops.

Another factor which should affect the size, number, distribution and type of loop is the occurance of plastic deformation during rapid quenching. The outer layers of the specimen cool more rapidly than the inner layers. Because of thermal expansion a temperature gradient from the surface to the center is always accompanied by stress. If this stress at any instant during cooling is above the yield then plastic flow will occur. Dislocations will be set in motion leaving vacancy clusters and perhaps even small dislocation loops in their wake. These may act as sinks for disappearance of thermal vacancies.

Takamura[4] has made careful dilatometric measurements on quenched gold specimens of various thickness. He concludes that in thin specimens the quenched in vacancy concentration corresponds to the freezable number of thermal vacancies that have been in equilibrium at quenching temperature. For thicker specimens, even though most of the thermal vacancies are lost due to the slower rate of cooling: still appreciable concentrations of vacancies can be observed. He suggests that a large number of vacancies can be generated during quenching. Because the production of these vacancies is due to plastic deformation during quenching and because the amount of plastic deformation increases with the increase in thickness, an appreciable fraction of the excess vacancies in thick quenched specimens may result from this cause.

The purpose of the present experiments was to obtain further information concerning the factors that affect the number, type, size and distribution

of loops that are observed in quenched and aged aluminum. In particular it seemed worthwhile to investigate the effect of quenching stress by studying the effect of specimen thickness on the substructure of quenched and aged pure aluminum and by comparing the substructure of two different orientations: {100} for which the four {111} planes are symmetrically oriented relative to specimen surface and {112} for which they are not.

Experimental Procedure

A. Specimen Preparation

{100} Samples

Polycrystalline 99.999% pure aluminum was rolled to thin plates of desired thickness namely 100μ, 125μ, 200μ, 300μ and 400μ. Strips (2.5 cm x 2.5 cm) were cut and annealed in air at 645°C for 24 hours to minimize dislocation density. This treatment gave a highly preferred [100] orientation with a grain size of 0.8 mm in diameter. Specimens 25μ thick were obtained by electropolishing annealed 100μ thick specimens.

{112} Samples

Single crystals (20 cm x 2.5 cm x .05 cm) were grown from polycrystalline 99.999% pure aluminum in vacuum. Graphite moulds packed with spectroscopic graphite powder were used for this purpose. Adjustment of the specimen thickness to the desired values (25μ, 125μ, 300μ, 400μ) was accomplished primarily by chemical polishing in the following solution at 90°C.

Phosphoric acid	(86%)	-800 c.c.
Sulphuric acid	(96%)	-120 c.c.
Nitric acid	(70%)	- 80 c.c.
Water		- 40 c.c.

However, careful mechanical polishing was necessary prior to chemical polishing. An attempt at chemical polishing of as-grown single crystals without mechanical polishing resulted in pitted specimens due to non-uniform attack on the surface. Mechanical polishing, however, removed the coating of oxide allowing uniform dissolution of the surface. A final electropolish was necessary to produce a smooth surface that proved to be more resistant

to the growth of a thick oxide layer during annealing. The electropolishing conditions were the same as discussed later. The specimens were then annealed in air at 645°C for 24 hours.

B. Quenching.

Annealed specimens were put in a specimen holder made of inconel (Fig. 18). The assembly was put into a quenching furnace containing a vertical slot (7.5 cm x 7.5 cm x 0.32 cm), maintained at a temperature of 543°C. Conventional tube furnace was not used for quenching because of the cooling that takes place during travel through the relatively long distance before reaching the quenching bath. The furnace was designed to bring the hot zone as close as possible to the quenching bath. Moreover, in the small slot, the temperature was uniform within ±5°. The size of the loop increases with decreasing quenching temperature and increasing water temperature. A relatively low quenching temperature (543°C) was chosen for these experiments in order to get large loops. A reduction of 33% excess vacancy is achieved by quenching from 543°C instead of 630°C. Therefore, decrease in quenching temperature results in less supersaturation of vacancies which means fewer nuclei of loops and more probability of getting larger loops.

The specimens were kept at 543°C for 45 minutes to ensure complete thermal equilibrium and quenched in water at 40°C which was also the aging temperature.

In order to minimize frictional forces on the specimen holder which might have reduced the speed of quenching, a 3 pound block of lead was used to pull the specimen holder through the quenching bath.

C. Aging.

All specimens were aged at 40°C for 5 minutes. This allowed the vacancies to cluster and to form dislocation loops.

D. Preparation of Electron Transparent Foils.

Quenched and aged specimens were electropolished at 0°C using an electrolyte of the following composition.

Perchloric acid	(70%)	- 110 c.c.
Ethyl Alcohol	(95%)	- 480 c.c.
Butyl Cellosolve		- 50 c.c.

The cellosolve increased the viscosity of the liquid, and thereby decreased the current density. Thus polishing could be carried out at 0°C instead of -30°C.

A stainless steel beaker which was used to hold the electrolyte also served as a cathode. The polishing was carried out at 10 volts, with a current density of 0.15 amp/cm^2.

A modified window method was employed to produce the electron microscope specimens. Near the end of the thinning process, the current was alternately switched on and off, causing small flakes suitable for transmission work to separate from the thin edges and fall to the bottom of the beaker. An advantage of this method is that it enables one, without the necessity of cutting operation, to get thin flakes of suitable dimensions to be placed on an electron microscope screen. The conventional technique in which specimens are cut from thin edges with a scalpel might cause deformation in the specimen. Plastic deformation during specimen preparation can certainly lead to confusion of the results.

The flakes were profusely washed with 100% ethyl alcohol to get a clean surface, free from any contamination. Surface contaimination can result from a layer of organometallic compounds which are formed during electropolishing. Deposits can often be left on the surface during drying of the alcohol unless care is taken to drain the solution from the areas of interest to promote quick drying.

E. Microscopic Examination.

A Siemens Elmiskop I electron microscope operated at 100 Kv was used to examine the specimens. The specimens were mounted on 75 mesh copper grids. The condenser aperture used was 400μ and useful beam current was 5μ A. Selected area diffraction and slip traces were used to determine the orientation and thickness of foil.

In general, precautions were taken at all stages not to deform the specimen. Any deformation might, for example, destroy the stacking faults in imperfect loops and cause perfect loops to glide to the surface of the foil.

Results and Interpretation

A. General features.

The results are shown as Figs. 1 to 6 ({100} oriented specimens) and Figs. 7 to 10 ({112} oriented specimens). It is clearly shown that even though all other important variables such as quenching temperature, aging temperature, and purity are kept constant, great differences in the resulting loop substructures can be caused simply by varying the thickness of specimens at the time of quenching. These differences will be described in detail in the following sections. Unfortunately changing the thickness during quenching probably affects the quenching conditions in several ways. The final thin foil that is observed is always from the central part of the original specimen.

(1) The maximum temperature difference from center to surface that occurs during quenching is greater for the thicker specimens. Therefore, stresses high enough to move dislocations within the central zone of the specimen are most likely to have existed in the thick specimens. If the temperature difference between center and surface becomes greater than about 1°C at any time during cooling then plastic relaxation will occur. If quenching deformation does take place, then residual stresses of the order of the yield stress may also be present during the aging treatment that follows quenching.

(2) The thickness must also affect the quenching rate. The cooling rate at the center of the specimen should decrease with increasing thickness.

(3) For very thin specimens (25μ) it is difficult to achieve such uniform flow of quenching water to the two sides of the foil that bending stresses are avoided. Therefore, some of these specimens may also be subjected to plastic deformation during quenching. Slight warping of the thinnest specimens was often caused by the quenching operation.

B. Effect of thickness at the time of quenching on average size loops, number of loops per unit volumes, and total excess vacancy concentration that appears as loops.

(1) Size and density vs. thickness.

Considerable variations in size and density of the loops were observed in specimens of different thickness. For identical quenching temperature and aging condition, the size of the loops progressively increased and their density decreased with increasing thickness of specimens.

An additional assumption was necessary to make an accurate estimate of loop density and thereby the vacancy concentration in foils which contained loops of relatively large size. The diameter of the loops became comparable to foil thickness in thicker specimens. Loops that intersected the top and bottom surfaces of the electron microscope specimen were almost never observed. This means that loops almost always glide to the surface and disappear whenever any part of the loop touches the specimen surface. Loops were therefore concentrated near the central zone of a foil. A correction factor D sin θ where D is the average true diameter of loops and θ is the angle which the habit plane of the loop makes with the foil surface was employed to estimate thickness in which observed loops were stable. True diameter of the loop can be measured from the micrographs because the longest diagonal parallel to <110> projects in true length when the beam is normal to foils of {100} and {112} orientation.

For the {100} orientation where four {111} planes are symmetrical, the correction D sin θ was the same for all sets of imperfect loops. For the {112} orientation, where {111} planes are asymmetrically oriented, different correction factors were necessary for the four families of

imperfect loops. These were D sin 19.5°, D sin 61.9°, and D sin 90° for 19.5°, 61.9° and 90° planes respectively designated as α, β, γ planes hereafter. In case of perfect loops, the habit plane was usually not known. A thickness correction equal to 0.7 times the average loop diameter was employed.

Figure 15b and 15c give the average diameter and density of the loop (corrected for the surface "loop free" zone) as a function of thickness of specimens quenched. The average diameter of loops in 25μ specimens was only 800 Å as compared to 4100 Å in 400μ thick specimens; on the other hand, 100μ specimens contained on an average 1.7×10^{13} loops/cm^3 while 400μ specimens had only 8×10^{12} loops/cm^3. Thus, quenching rate or quenching stress apparently play an important role in determining the size and density of loops.

(2) Vacancy concentration needed to account for loops.

Another parameter that might change with specimen thickness is the total excess vacancy concentration that finally appears in the form of loop. In particular it might be expected that in the thinnest specimens some of the excess vacancies even from the central part of the specimen might be lost to the external surfaces. In thicker specimens some vacancies might be lost to other sinks such as dislocation lines. The excess vacancy concentration can be calculated from corrected loop density and average loop diameter if the thickness of the foil at the area under observation is known. The results are shown in Table I for {100} oriented specimens and Table II for {112} oriented ones.

The concentrations of vacancies were calculated assuming that loops were formed by one layer of vacancies in {111} planes and the foil thickness

was 4000 Å. All photographs in which slip traces occurred were found to have a thickness close to 4000 Å. However, the fact that slip traces were not present for all photographs used, means that errors as much as a factor of 2 may have been made in assuming the thickness to a first approximation as 4000 Å. The results show that the total number of excess vacancies which finally appear in the form of loops was independent of quenching thickness.

C. Effect of quenching thickness on the relative number of faulted and perfect loops.

Examination of the microstructures (Figs. 1 to 10), revealed that in 125μ thick specimens the loops were almost all Frank loops. In thicker specimens both faulted and perfect prismatic diamond shaped loops were observed. The percentage of perfect loops increased with increasing thickness at the time of quenching as shown in Fig. 15a. The thickest specimens (400μ thick) contained almost all perfect loops.

D. Transformation of loops due to stress.

During observation in the electron microscope, some of the stacking fault type loops were transformed into perfect prismatic loops. Therefore, local stresses due to heating of the electron beam or due to carbon deposition were sufficient to aid in nucleating a Shockley partial which swept away the stacking fault. Figure 11a and 11b show that loop A had lost its stacking fault fringes.

E. Prismatic gliding.

Gliding of perfect dislocation loops was frequently observed during microscopic observation. Figure 11a and 11b shows the glide to the surface of a transformed loop B leaving behind hexagonal trace B'. The loop B, originally a Frank sessile, had a Burgers vector $\frac{1}{3}[\bar{1}11]$. After transformation it became a perfect loop on $(\bar{1}11)$ plane with a Burgers vector $\frac{1}{2}[\bar{1}01]$. It moved to the surface along $[\bar{1}01]$.

F. Interaction of prismatic loops.

During glide two or more prismatic loops sometimes came close enough to cause coalescence. Two cases could be distinguished.

(1) If the Burgers vectors were the same the portions of the two loops which met would annihilate forming a single loop (Fig. 6b).

(2) Loops having different Burgers vectors formed nodes. In Fig. 14 loop B having a Burgers vector $\pm \frac{1}{2}[011]$ was in poor contrast. Since the operating reflection was 200 for which $\vec{g}\cdot\vec{b}=0$. Loop A might have any of the following Burger vectors $\pm \frac{1}{2}[110]$, $\pm \frac{1}{2}[101]$, $\pm \frac{1}{2}[\bar{1}10]$, $\pm \frac{1}{2}[\bar{1}01]$, $\pm \frac{1}{2}[1\bar{1}0]$. Thus the dislocation 'C', which could have a Burgers vector $\frac{1}{2}[110]$ formed by a reaction of the type

$$\frac{1}{2}[011] + \frac{1}{2}[10\bar{1}] = \frac{1}{2}[110]$$

G. Observations on {112} orientation.

Observations in specimens of {112} orientation agreed generally with those in {100} orientation. As in {100} orientation the type, size, number and distribution of the loops seemed to be strongly dependent on

thickness of specimen quenched, i.e., on quenching rate and stress. Figure 8 for 125μ thick specimens showed all faulted loops. Figure 9 for 300μ specimens showed a combination of diamond shaped and faulted loops while Fig. 10 for 400μ thickness showed predominantly perfect diamond shaped loops. Figures 13a and 13b represent typical substructures of quenched and aged 125μ foil at a higher magnification. It consisted of 4 distinct sets of faulted loops. The edge-on loops A were on γ plane, loops B on α plane and loops C and loops D on the β planes respectively.

In the thinnest specimens 25μ, Fig. 7, almost all loops observed were faulted. This was interesting because in absence of deformation, all specimens with thickness below the critical value (125μ) should consist of a substructure containing all faulted loops.

H. Distribution of loops among possible orientations.

(1) Imperfect loops.

The distribution of imperfect loops on four {111} habit planes was uniform in {100} oriented specimens. In {112} specimens where the {111} planes are not symmetrical with respect to the specimen surface uniform distribution of loops between {111} planes were also observed. The relative numbers of loops on four {111} planes are given below. These numbers have been corrected for the different effective thickness of the foil for the planes as previously discussed.

loops on 19.5° plane	$\simeq 3 \times 10^{12}$ loops/cm^3
loops on 61.9° plane	$\simeq 2 \times 10^{12}$ loops/cm^3
loops 90° plane	$\simeq 2.1 \times 10^{12}$ loops/cm^3

(2) Perfect loops.

Figure 6 and Figure 12 show the preferred orientation of diamond shaped perfect loops along <100> direction. The habit plane of diamond shaped loops was very close to {023}. Therefore, at least 8 families of diamond shaped loops should be visible in {100} orientation if all 16 of {023} planes were equally populated. Frequently only 2 or 3 types of diamond shaped loops were found. This strongly preferred orientation suggests that movement of dislocations due to quenching stress may be responsible for the nucleation of diamond shaped loops. The loops may have the same Burgers vector as the dislocations that moved in that particular region during quenching. Moving dislocations are known to leave behind small prismatic loops. These might act as sinks for the excess vacancies.

I. Habit plane of perfect diamond shaped loops.

Figure 6b was a typical substructure containing diamond-shaped loops. From the faulted loops that are present it is possible to accurately determine the orientation of crystallographic axes relative to the plane of the photograph. If it is assumed that the sides of perfect diamond shaped loops lie in {111} planes then it is possible to estimate their habit planes. Four different sets of perfect loops can be seen in this photograph. In projection loops A were wide while other loops B that had the same direction of major diagonal were narrower. Loop C and loop D were edge-on. Analysis showed that although loop C and loop D were seen edge-on they were about 10° off from {110} or about on {320}. The habit plane of loops A and B was also determined. Figure 16 showed a typical

glide cylinder enclosed by (111) and ($\bar{1}1\bar{1}$) planes. The shortest dislocation line length for a given perfect loop occurs when the sides are along [$\bar{1}2\bar{1}$] and [121]. That is, the loop lies on the (10$\bar{1}$) plane. The directions of long and short diagonal would be [010] and [101] respectively. Because the foil orientation is [100] the projection of the loop onto (100) must be considered. Taking the long diagonal (which would be parallel to [100]) as unity, the projected length of the shorter diagonal should be 0.5. A loop on (101) plane should have a ratio of short to long diagonal of .5. Loops A and loops B had a ratio of short to long diagonal of .6 and .4. Therefore, these loops are also rotated away from the exact ($\bar{1}$01) orientation to opposite sides of ($\bar{1}$01). The shapes can be explained if they were rotated by about 10° as shown in Fig. 17. For both wide and narrow loops the direction of the long diagonal was exactly [010]. This means that rotation had taken place about the [010] axis and the habit planes of loops A and loops B were also close to {320}. Therefore, perfect diamond shaped loops were near {110} but rotated away about 10° toward {100} rather than toward {111}. The latter might be expected if they had originally grown on {111} and then moved by glide to shorten the total length of dislocation line. Makin and Hudson,[21] Westmacott et. al[22] and Embury and Nicholson[23] have also reported a similar observation. They found an {012} habit plane.

Kuhlmann-Wilsdorf and Wilsdorf[8] suggested that diamond shaped loops lay on {110} planes having sides along <112> directions. They also suggested that this kind of loop had either been nucleated or at least grown on {110}. Thomas and Eikum[19] and Thomas and Washburn[20] discussed the formation of diamond shaped loop on the basis of combined glide and

climb of a hexagonal perfect loop originally lying on {111}.

Alternatively the habit plane of diamond shaped loops might not be {110} due to elastic interaction between opposite sides of the loop. The {023} or {012} orientation might actually be one of lower energy than {011} for a diamond shaped loop with all four sides lying on {111} planes. No exact calculations have been made for this case.

Summary and Conclusion

It has been shown that great differences in substructure of quenched and aged aluminum can be caused by varying the thickness of the specimen that is quenched even though all other important variables like quenching temperature, aging temperature and time, and purity are kept constant.

In thicker specimens, stresses high enough to cause plastic deformation may be developed during quenching. The dislocations that move due to these stresses may leave behind small perfect loops or dislocation dipoles that can act as nuclei for (the growth of large) perfect loops. In thinner specimens, quenching stresses may not have been great enough to move large numbers of dislocations. Homogeneous nucleation apparently leads to the growth only of stacking fault loops. The presence of numerous perfect loops in some of the very thinnest specimens quenched may be due to deformation caused by mechanical bending stresses during entrance of the 25μ thick foils into the quenching bath. Foils approximately 125μ thick consistently contained almost exclusively faulted loops. The results suggest that this thickness resulted in the best compromise between deformation by quenching stresses and deformation due to bending. The following is a summary of the most important findings:

(1) The size of the loops progressively increases and their density decreases with increasing thickness of specimens. For identical quenching temperature and aging conditions, the average diameters and densities of loops were 800 Å, 1.7×10^{13} loops/cm^3 and 4100 Å, 8×10^{12} loop/cm^3 for 25μ and 400μ thick specimens respectively.

(2) The concentration of vacancies that was necessary to account for the size and density of loops was of the order of 10^{-5} and approximately independent of specimen thickness.

(3) Loops that intersected the top and bottom surfaces of the electron-transparent foil were almost never observed; they apparently always glided to the surface and disappeared creating loop free zones near the surfaces.

(4) Quenched specimens of the intermediate thickness value approximately 125μ, contained almost entirely faulted loops. The percentage of perfect loops increases with increased thickness of the specimen above 125μ. 400μ thick specimens contained almost all perfect loops. Large perfect loops were usually diamond shaped.

(5) The diamond shaped perfect loops had an orientation near {023} planes. Usually all those in a neighboring region had the same habit plane.

(6) The distribution of imperfect loops among the four habit planes was uniform.

Acknowledgements

The author expresses his gratitude to Professor Jack Washburn for his encouragement, patience and continued interest and to Professor Gareth Thomas for his helpful discussions. This work was supported by the auspices of the U.S. Atomic Energy Commission through the Inorganic Materials Research Division of the Lawrence Radiation Laboratory.

References

1. F. J. Bradshaw and S. Pearson, Phil. Mag., 2, 379, 570 (1957).
2. T. Federighi, Phil. Mag., 4, 502 (1959).
3. W. De Sorbo and D. Turnbull, Acta Met., 7, 83 (1959).
4. J. Takamura, Acta Met., 9, 547 (1961).
5. M. Meshii and J. W. Kauffman, Acta Met., 7, 180 (1959).
6. R. Maddin and A. H. Cottrell, Phil. Mag., 46, 735 (1955).
7. F. C. Frank, Symposium on the Plastic Deformation of Crystalline Solids, (Carnegie Institute of Technology, Pittsburgh, 1950).
8. D. Kuhlmann-Wilsdorf and H. G. F. Wilsdorf, J. Appl. Phys., 31, 516 (1960).
9. J. Galligan and J. Washburn, Phil. Mag., 8, 93, 1455 (1963). Also Lawrence Radiation Laboratory Report Number 10606 Rev.
10. K. Chik, A. Seeger and M. Ruhle, Proc. 5th Int. Congress Electron Microscopy, Academic Press (1962), p. J-11.
11. D. Kuhlmann-Wilsdorf, Phil. Mag., 3, 125 (1958).
12. P. B. Hirsch, J. Silcox, R. E. Smallman and K. H. Westmacott, Phil. Mag., 3, 897 (1958).
13. P. B. Hirsch and J. Silcox, Phil. Mag., 4, 72 (1959).
14. R. Vandervoort and J. Washburn, Phil. Mag., 5, 24 (1960).
15. R. M. J. Cotterill and R. L. Segall, Phil. Mag., 8, 1105 (1963).
16. S. Yoshida, M. Kiritani and Y. Shimomura, J. Phys. Soc. Japan, 18, 175 (1963).
17. J. L. Strudel and J. Washburn, Phil. Mag., in press. Also Lawrence Radiation Laboratory Report Number 10959.
18. G. Saada, J. Phys. Soc. Japan, 18, (III) 41 (1963).

19. G. Thomas and A. Eikum, J. Appl. Phys., 34, 3363 (1963). See also Lawrence Radiation Laboratory Report Number 10814.

20. G. Thomas and J. Washburn, Rev. Mod. Phys., 35, 992 (1963). See also Lawrence Radiation Laboratory Report Number 10674.

21. M. J. Makin and B. Hudson, Phil. Mag., 8, 447 (1963).

22. K. H. Westmacott, R. S. Barnes, D. Hull, R. E. Smallman, Phil. Mag., 6, 829 (1961).

23. J. D. Embury and R. B. Nicholson, Acta Met., 11, 347 (1963).

Figure Captions

Figures 1 to 6 show typical substructures of Al (99.999%) specimens of {100} orientation, quenched from 543°C and aged 5 minutes at 40°C.

Fig. 1. (a), (b), (c), (d): The typical substructures of 25μ thick specimens. Loops are of perfect prismatic type. The average diameter of the loops is 850 Å.

Fig. 2. (a), (b), (c), (d): The substructures of 100μ thick specimens. Notice increased density of loops of the average diameter of 1250 Å.

Fig. 3. (a), (b), (c), (d): The substructures of 125μ thick specimens. Note all Frank sessile loops contain stacking fault fringes. The average diameter of the loops is 1750 Å.

Fig. 4. (a), (b), (c), (d): The substructures of 200μ thick specimens. A combination of perfect and imperfect loops is seen. The average diameter of the loops is 2050 Å. Notice decreased density of loops.

Fig. 5. (a), (b), (c), (d): The substructures of 300μ thick specimens. Note increased percentage of perfect loops and decreased density of loops. The average diameter of loops is 3100 Å.

Fig. 6. (a), (b), (c), (d): The substructure of 400μ thick specimens. Note well developed diamond shaped loops of average diameter of 4100 Å.

The Figs. 7 to 10 show representative substructures of Al (99.999%). Specimens of {112} orientation under identical quenching and aging conditions.

Fig. 7. (a), (b), (c), (d): The substructures of 25μ thick specimens. Approximately 80% of the loops are faulted in nature with an average size of 1450 Å.

Fig. 8. (a), (b), (c), (d): The substructures of 125μ thick specimens, containing almost all Frank sessile loops with an average diameter of 2000 Å.

Fig. 9. (a), (b), (c), (d): The substructures of 300μ thick specimens. Notice combination of perfect and imperfect loops with average diameter of 2500 Å.

Fig. 10. (a), (b), (c), (d): The substructures of 400μ thick specimens. Almost all the loops are perfect prismatic with an average diameter of 2200 Å.

Fig. 11. (a), (b): Transformation of faulted loops into perfect prismatic loops during observation of foils. The loop A (Fig. 11a) has lost its stacking fault fringes (the loop A' in Fig. 11b) due to local stresses developed as a result of heating of the electron beam. The gliding of the loop B after transformation into perfect prismatic loop.

Fig. 12. (a), (b): The preferred orientation of diamond shaped loops in [100] direction.

Fig. 13. (a), (b): The typical substructure of quenched and aged 125μ foil at a higher magnification. It consists of 4 distinct sets of faulted loops.

Fig. 14. Interaction of perfect prismatic loops:
The loop B having a Burgers vector $\pm \frac{1}{2}[001]$ is in poor contrast, since the operation reflection is 200 for which $\vec{g}\cdot\vec{b} = 0$. The loop A is in contrast. The dislocation 'c' is formed as a result of interaction.

Fig. 15. (a). The plot shows the effect of quenching thickness on relative numbers of faulted and perfect loops.
(b). The plot represents the effect of quenching thickness on the average size of the loops.
(c). The plot illustrates the effect of quenching thickness on the density of loops in {100} orientation.

Fig. 16. A typical glide cylinder for the diamond shaped loops.

Fig. 17. The projection of a diamond shaped loop having the four-sides lying on {111} planes.
(1) The ratio of short to long diagonal for the wider loop A.
(2) The ratio of short to long diagonal for a loop of exact {110} orientation.
(3) The ratioof short to long diagonal for the narrower loop B.

Fig. 18. The inconel specimen holder.

Table I

Orientation of foil	Thickness of foil in μ	Average diameter of loops in Å	Correction Factor D sin θ in Å	Corrected thickness in Å	Average no. of loops	Area under observation	Concentration of vacancy
{100}	25μ	800 Å	650	3350	160	8.7×10^5 sq. Å	2.64×10^{-6}
	100μ	1250 Å	1020	2980	400	8.7×10^5 sq. Å	1.8×10^{-5}
	125μ	1750 Å	1428	2572	180	8.7×10^5 sq. Å	1.8×10^{-5}
	200μ	2050 Å	1675	2325	150	8.7×10^5 sq. Å	2×10^{-5}
	300μ	3100 Å	2530	1470	112	8.7×10^5 sq. Å	3.5×10^{-5}
	400μ	4100 Å	3350	650	40	8.7×10^5 sq. Å	2.8×10^{-5}

UCRL 11188

Table II

Foil Orientation	Specimen Thickness in μ	Average Diameter of Loops in Å	Concentration of Vacancy			Total Concentration Cv
			Cα	Cβ	Cγ	
{112}	25μ	1450 Å	3.3×10^{-6}	5.7×10^{-6}	2.6×10^{-6}	1.16×10^{-5}
	125μ	2000 Å	1.35×10^{-5}	3.1×10^{-6}	1.16×10^{-5}	2.82×10^{-5}
	300μ	2500 Å	1.4×10^{-5}	1.18×10^{-5}	1.25×10^{-5}	3.83×10^{-5}
	400μ	2200 Å				2.6×10^{-5}

Correction Factor			Correction Thickness			No. of Loops		
D sin 19.5	D sin 61.9	D sin 90	Tα in Å	Tβ in Å	Tγ in Å	nα	nβ	nγ
480	1280	1250	3520	2720	2550	64	86	36
660	1760	2000	3340	2240	2000	130	20	68
825	2200	2500	3175	1800	1500	55	37	34
				2500			150	

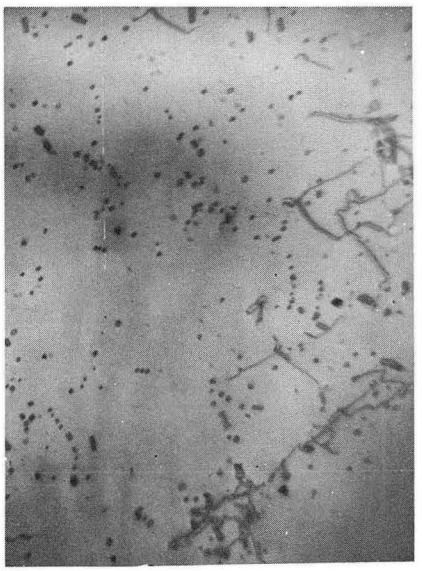

FIG. Ia

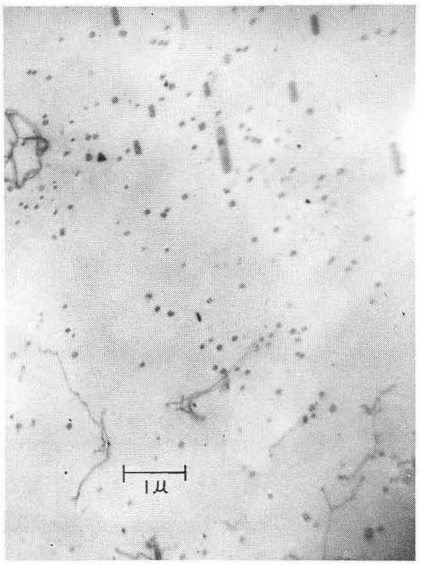

FIG. Ib

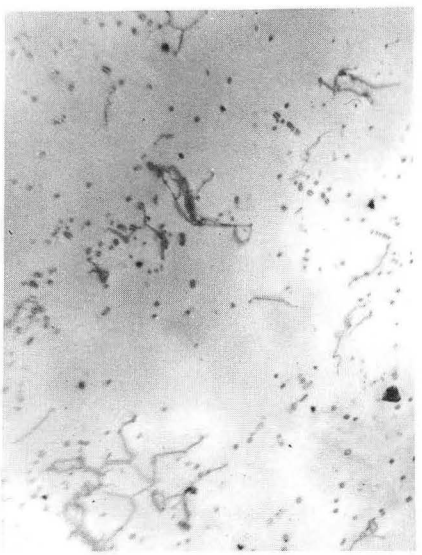

FIG. Ic

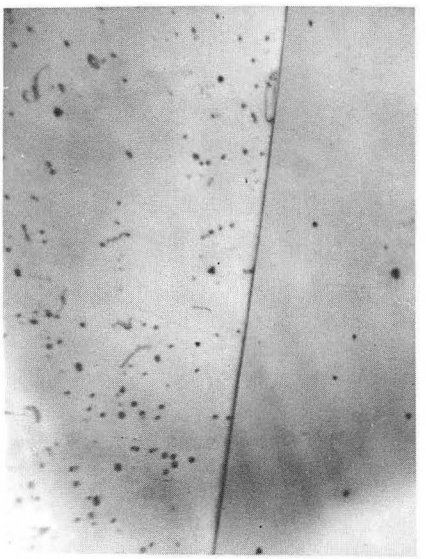

FIG. Id

ZN-4160

Fig. 1

FIG. 2a

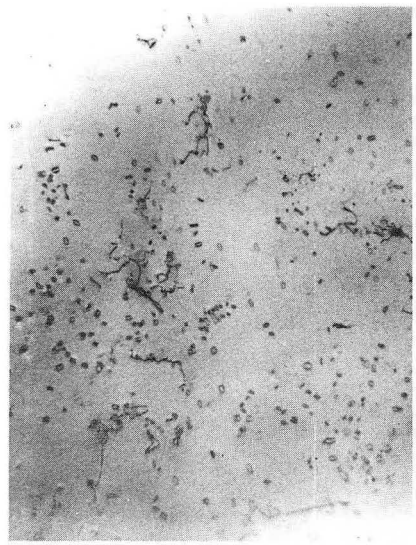

FIG. 2b

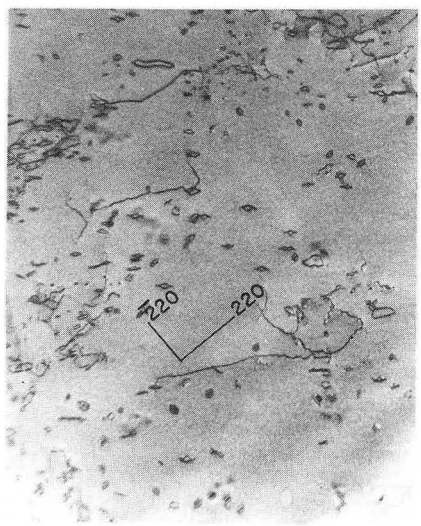

FIG. 2c

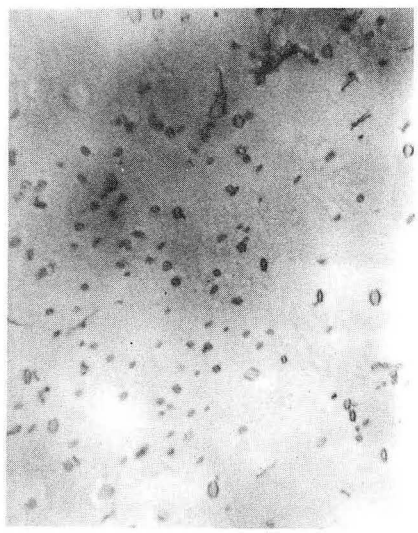

FIG. 2d

ZN-4161

Fig. 2

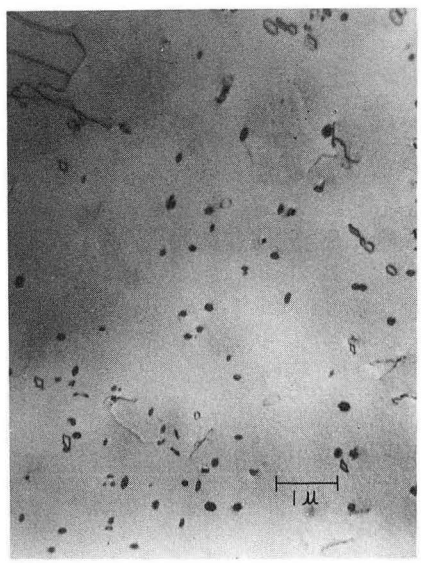

FIG. 3a

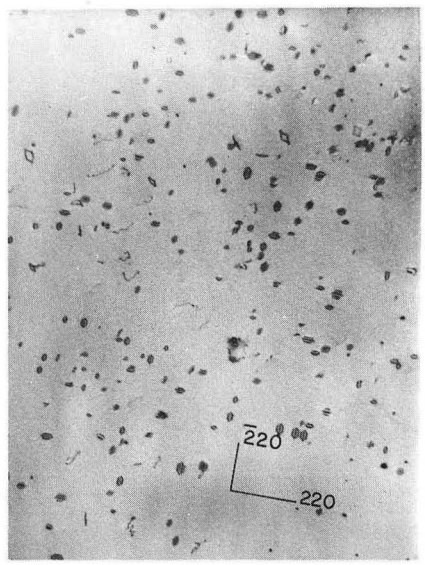

FIG. 3b

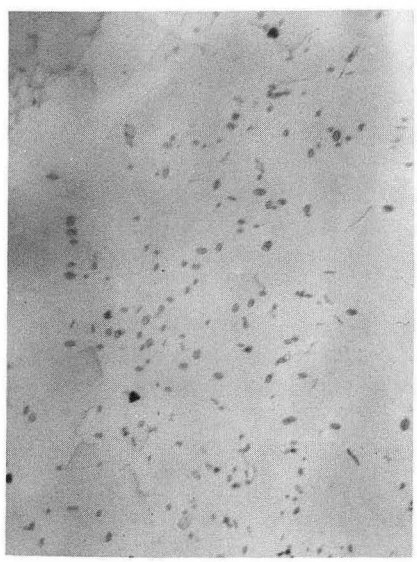

FIG. 3c

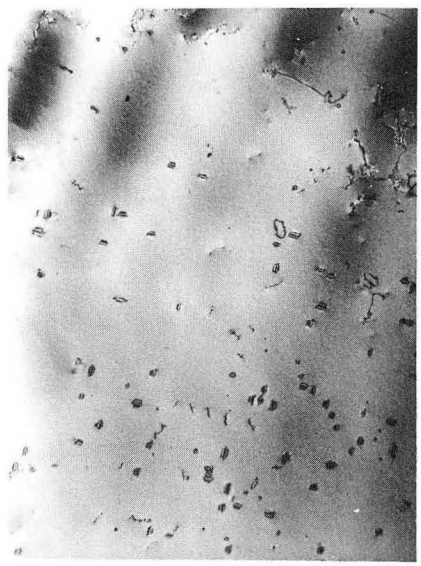

FIG. 3d

ZN-4162

Fig. 3

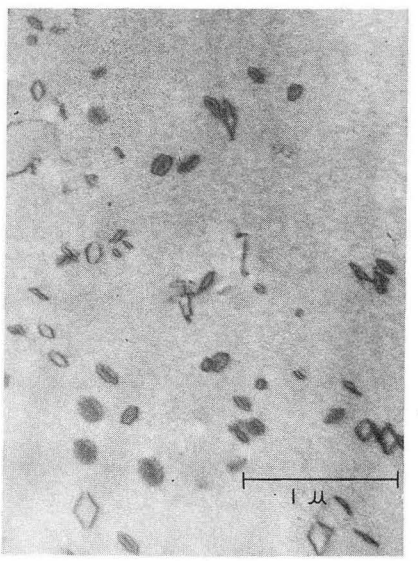

FIG. 4a

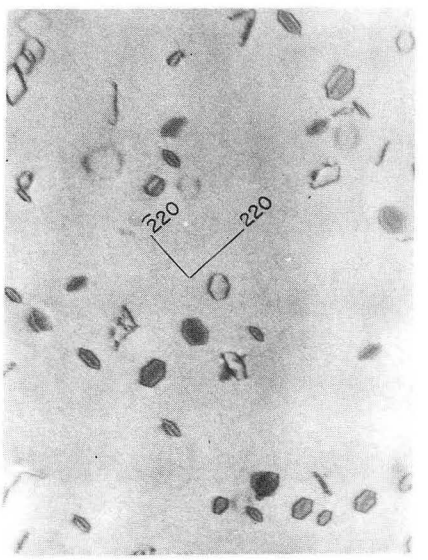

FIG. 4b

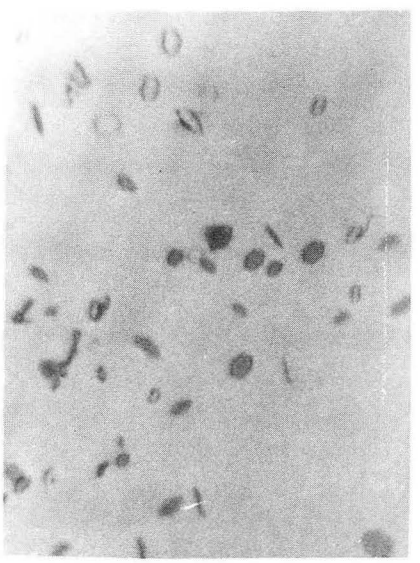

FIG. 4c

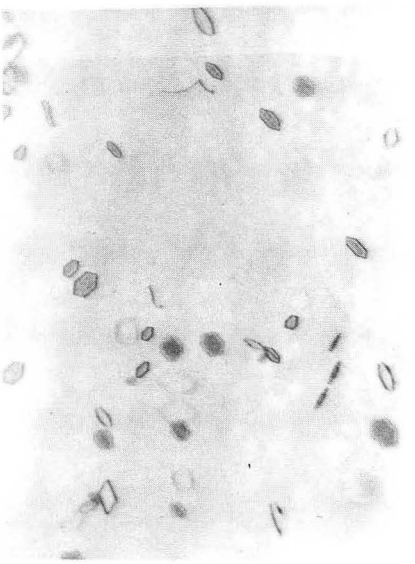

FIG. 4d

ZN-4163

Fig. 4

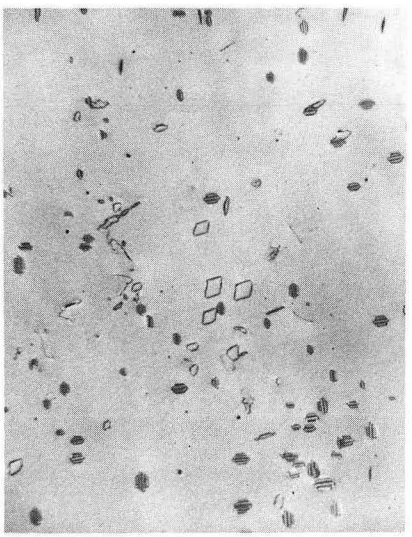

FIG. 5a

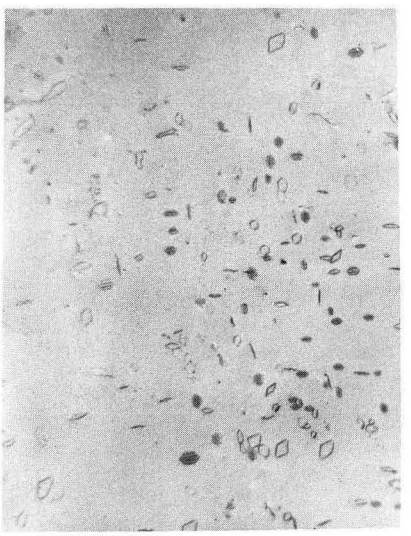

FIG. 5b

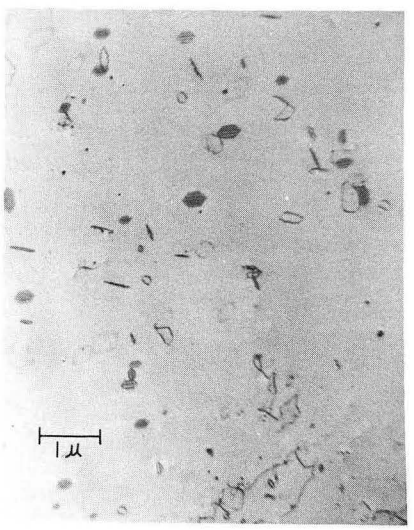

FIG. 5c

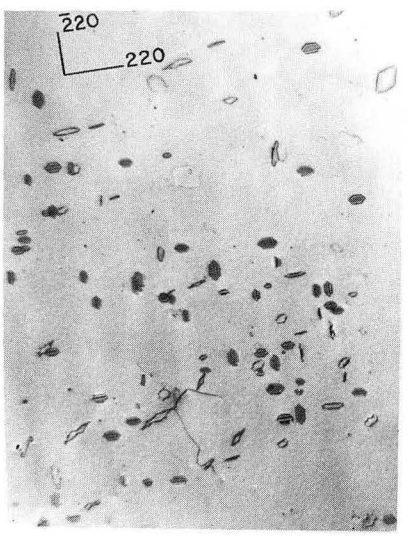

FIG. 5d

ZN-4164

Fig. 5

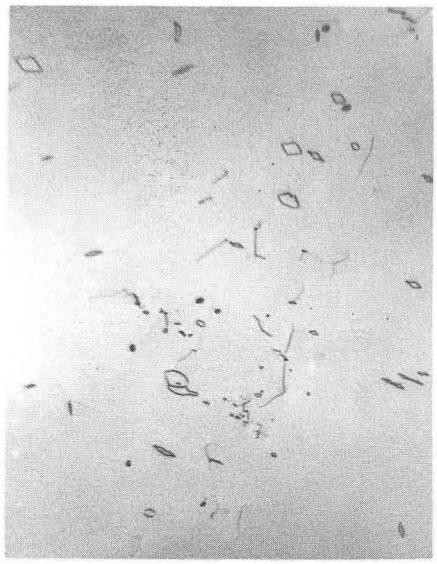

FIG. 6a

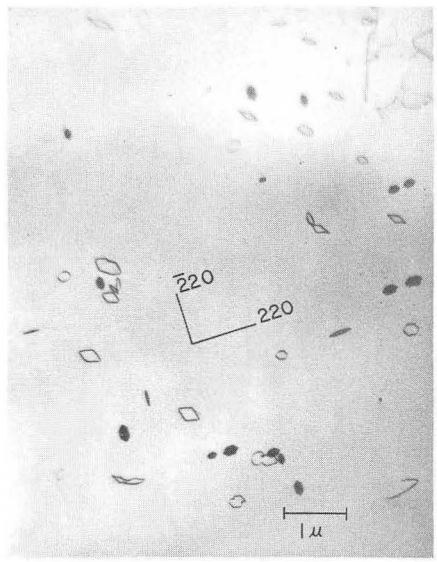

FIG. 6b

FIG. 6c

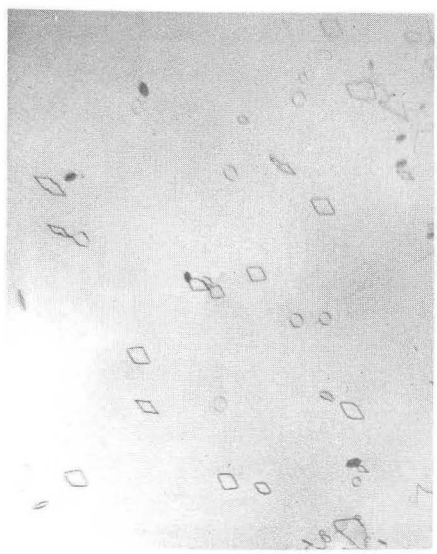

FIG. 6d

Fig. 6

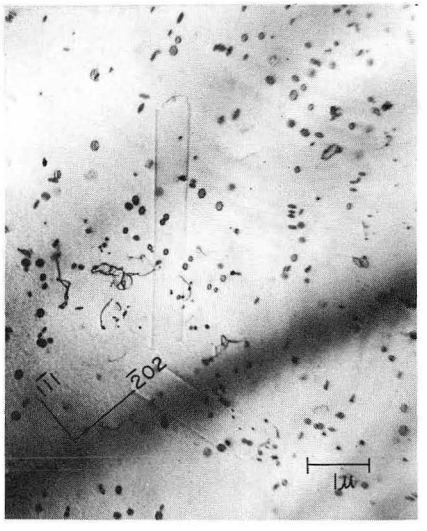

FIG. 7a

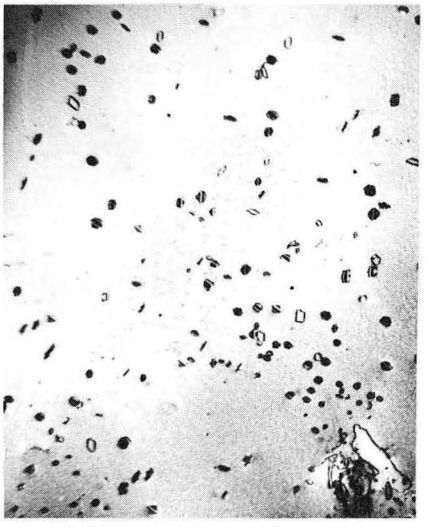

FIG. 7b

FIG. 7c

FIG. 7d

ZN-4166

Fig. 7

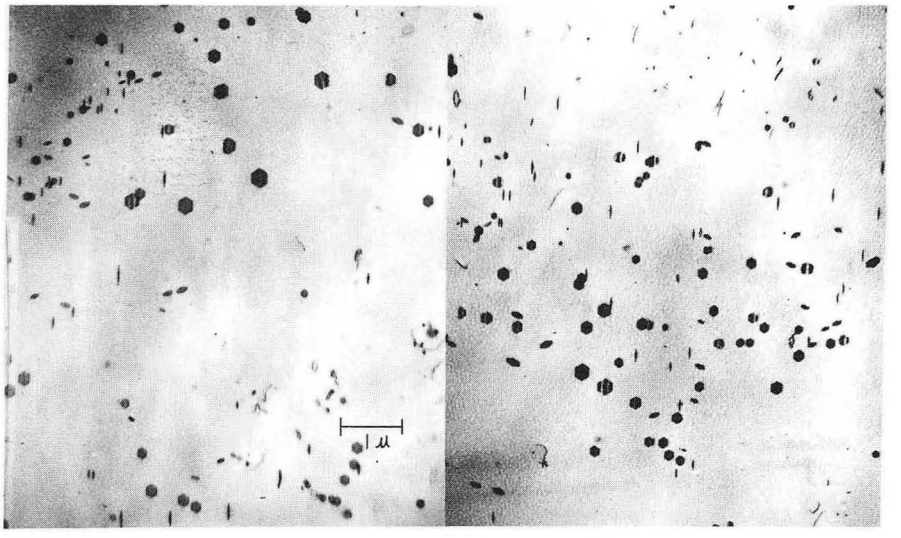

FIG. 8a

FIG. 8b

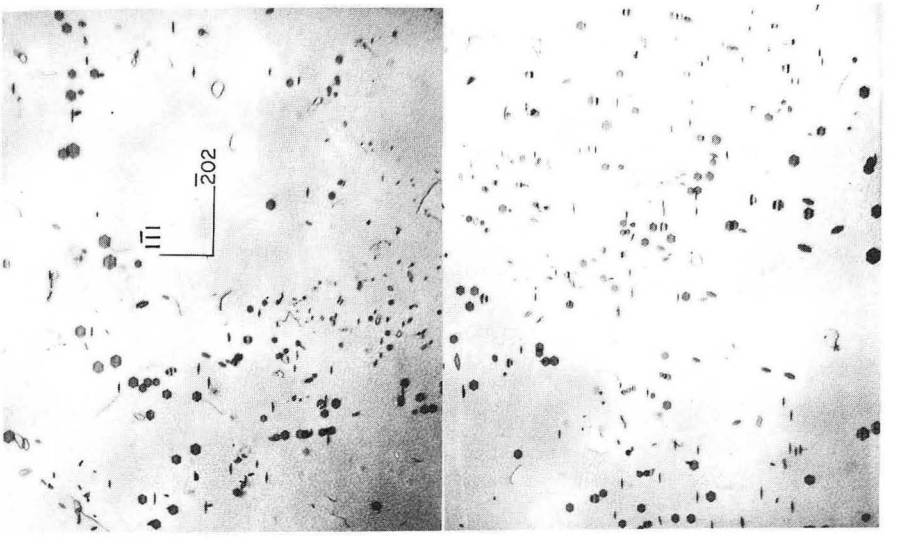

FIG. 8c

FIG. 8d

ZN-4167

Fig. 8

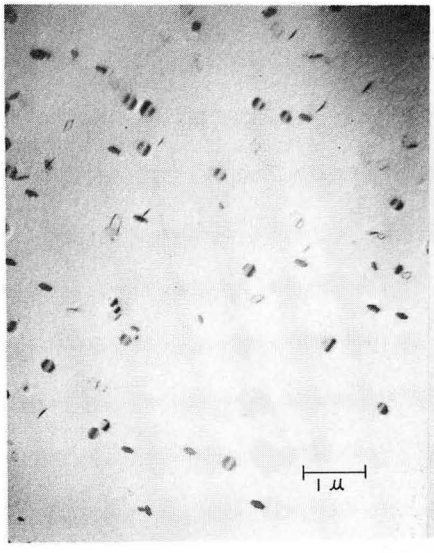

FIG. 9a

FIG. 9b

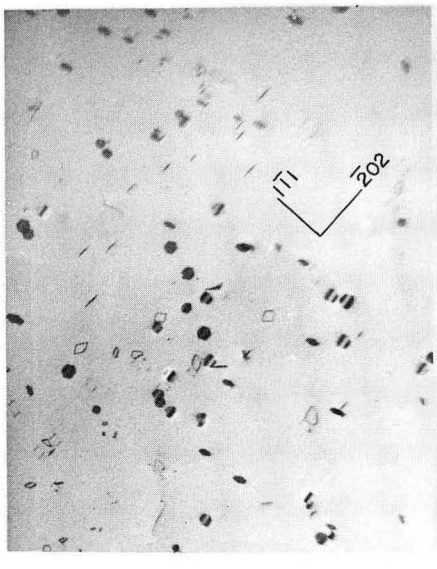

FIG. 9c

FIG. 9d

ZN-4168

Fig. 9

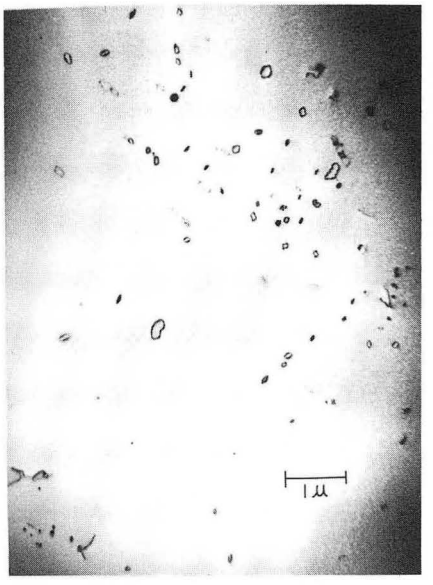

FIG. 10a

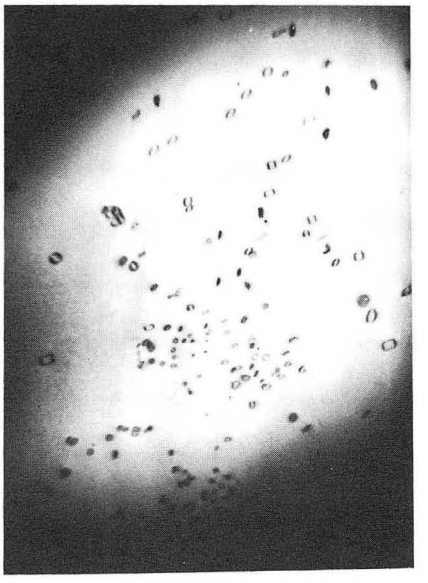

FIG. 10b

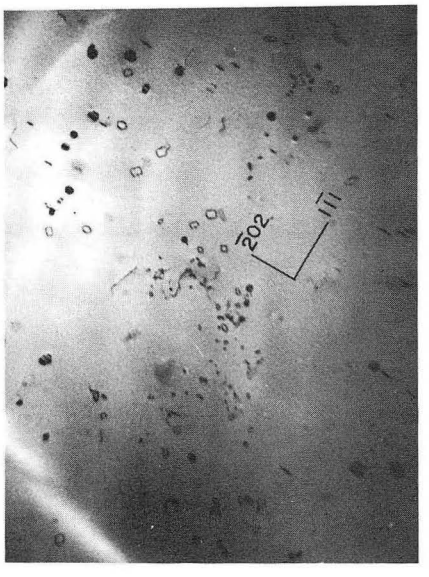

FIG. 10c

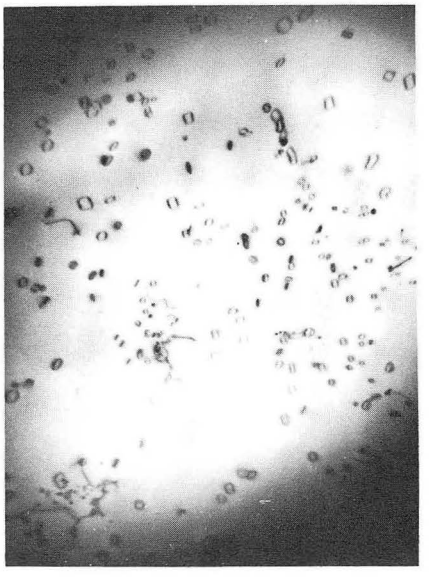

FIG. 10d

ZN-4169

Fig. 10

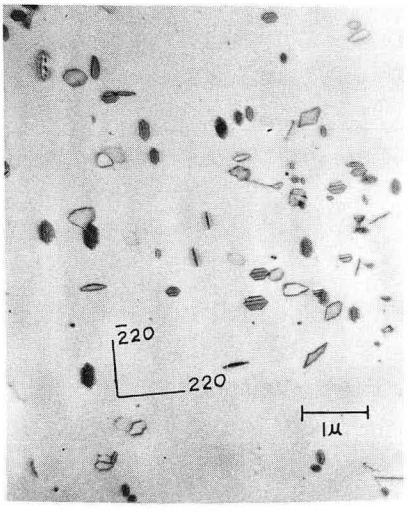

FIG. 11a

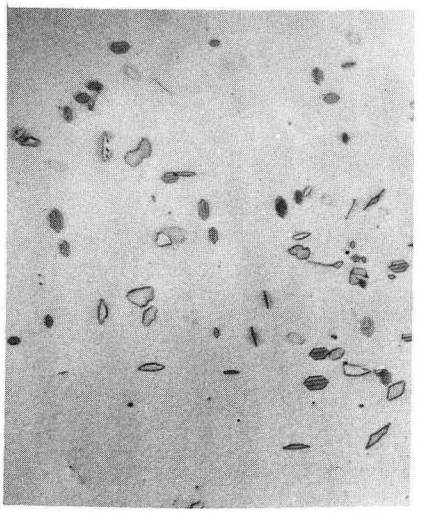

FIG. 11b

ZN-4170

Fig. 11

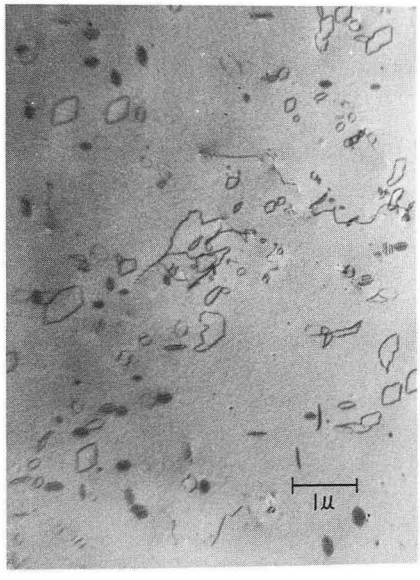

FIG. 12a

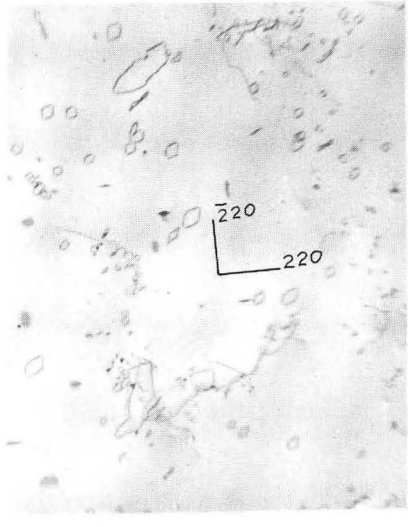

FIG. 12b

ZN-4171

Fig. 12

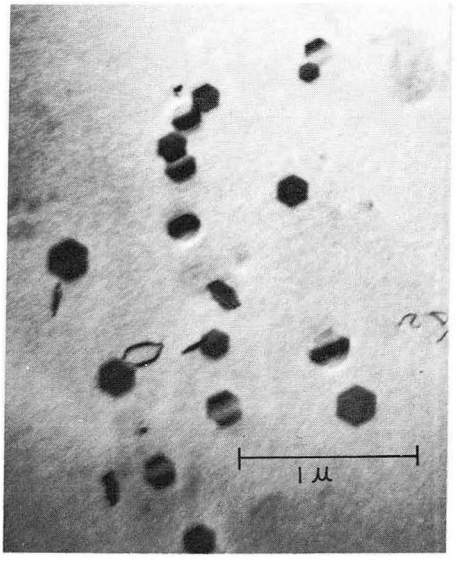

FIG. 13a

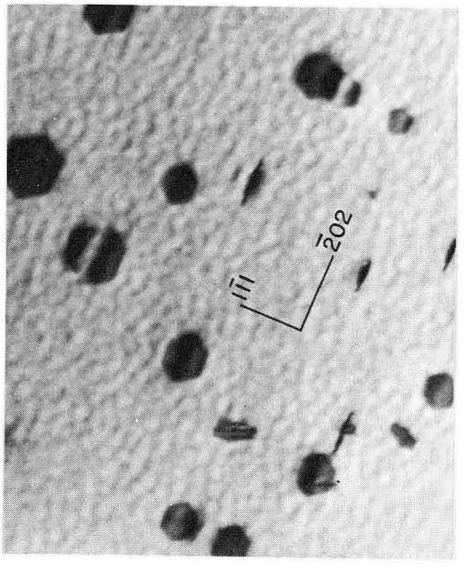

FIG. 13b

ZN-4172

Fig. 13

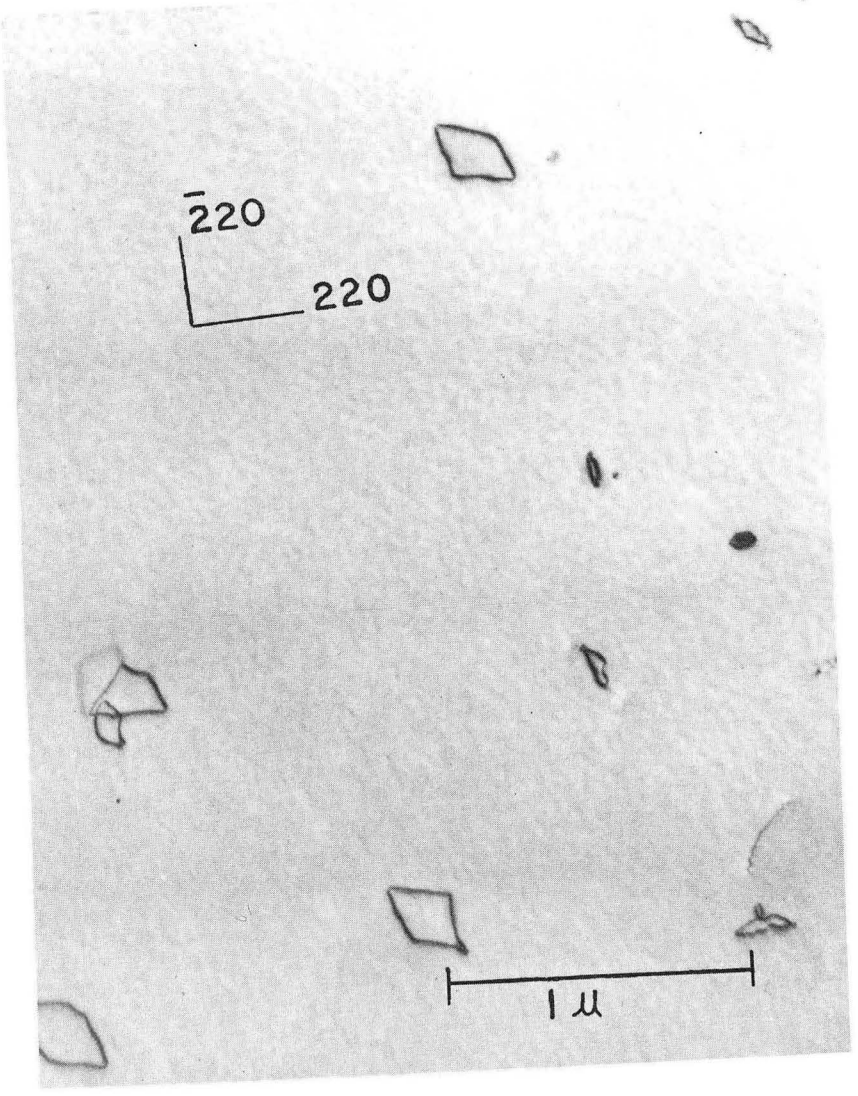

FIG. 14

ZN-4173

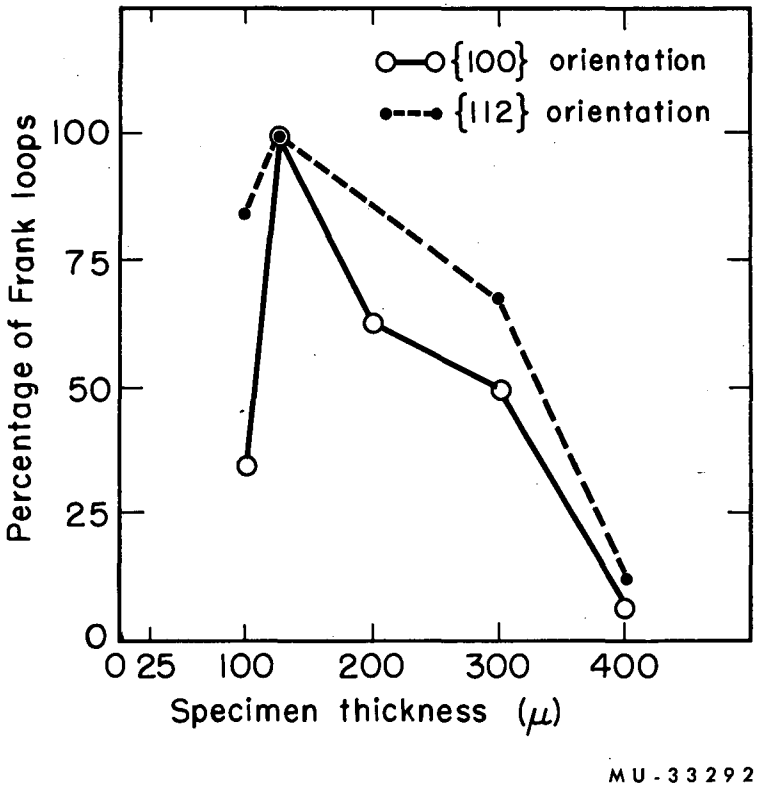
{100} orientation
{112} orientation
Percentage of Frank loops
100
75
50
25
0
0 25
100
200
300
400
Specimen thickness (μ)
MU-33292

Fig. 15a

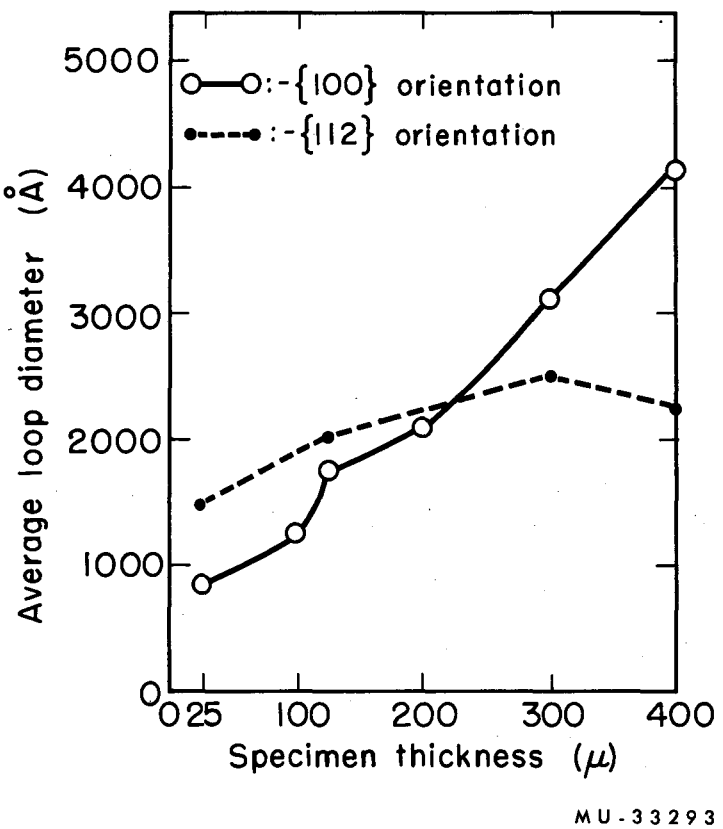
5000
4000
3000
2000
1000
0
Average loop diameter (Å)
O:-{100} orientation
:-{112} orientation
0 25 100 200 300 400
Specimen thickness (μ)
MU-33293

Fig. 15b

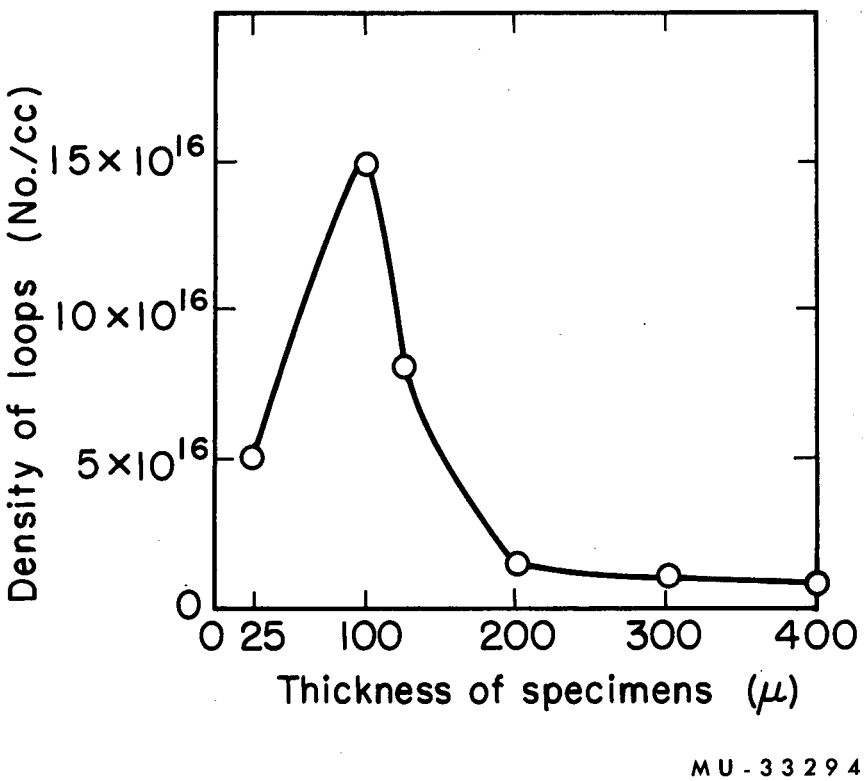
Density of loops (No./cc)
15×10^16
10×10^16
5×10^16
0
0 25 100 200 300 400
Thickness of specimens (μ)
MU-33294

Fig. 15c

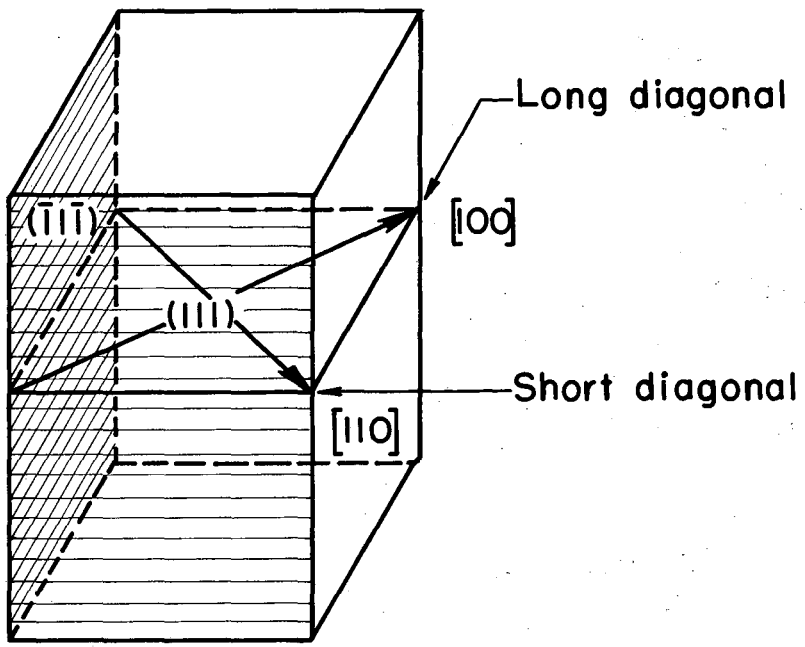

Fig. 16

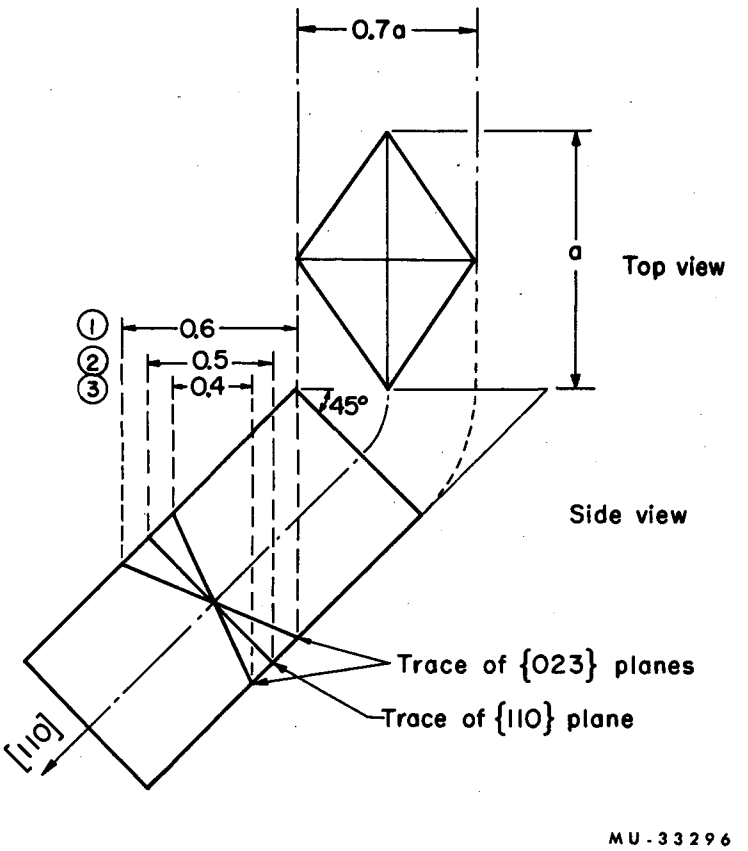
0.7a
a
Top view
1
2
3
0.6
0.5
0.4
45°
Side view
Trace of {023} planes
Trace of {110} plane
[110]
MU-33296

Fig. 17

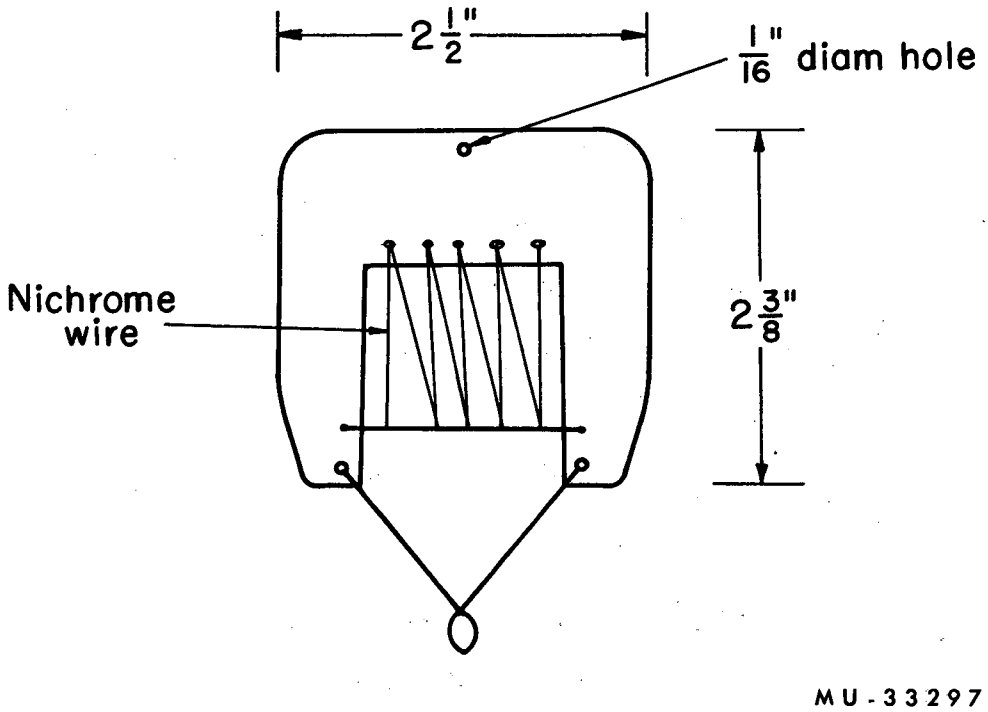

Fig. 18